RSC Advances

PAPER

View Article Online
View Journal | View Issue

Cite this: *RSC Adv.*, 2025, **15**, 41471

Anilino-carbazole-based D–π–D′–π–D blue light material coordinated exciplex for achieving white light dynamic regulation

Xiaoling Xie,[ab] Junfeng Wang,[b] Haocheng Zhao,[c] Zhenrui Gao,[b] Lei Yan,[b] Yuling Wu *[b] and Yanqin Miao *[b]

An exciplex white light system that can simplify the structure of a device has become an important driving force for the industrialization of white organic light-emitting devices (WOLEDs). Two D–π–D′–π–D-type blue light materials, **CzPAF-DPA** and **CzPAF-DF**, based on a core aniline-based carbazole and 9,9-dibutylfluorene as a π bridge with two peripheral donors with varying degrees of conjugation were successfully synthesized by Buchwald–Hartwig amination. Both materials emit blue light and are thermally stable, with thermal decomposition temperatures (T_d) of 408 and 418 °C, respectively. The electroluminescence (EL) spectra of both **CzPAF-DPA** and **CzPAF-DF** represented broad-band emission with two primary emission peaks. The shorter-wavelength peaks located at 424/428 nm correspond to the intrinsic emission peak of blue light materials, while the longer-wavelength peaks at 496/500 nm are ascribed to an exciplex generated at the interface between the light-emitting layer and the electron transport layer (ETL). By adjusting the thickness of the light-emitting layer, **CzPAF-DPA**, a controllable transition from warm white light to cold white light emission was achieved in single-molecule devices fabricated by both vacuum evaporation deposition and wet spin-coating. This research provides a crucial theoretical basis for developing blue light devices compatible with multi-process techniques, and promoting a method for the practical application of OLEDs in printed displays.

Received 18th June 2025
Accepted 4th October 2025

DOI: 10.1039/d5ra04330a

rsc.li/rsc-advances

1 Introduction

White organic light-emitting devices (WOLEDs), as a new generation of solid-state lighting technology, have shown great application prospects in the fields of healthy lighting and full-color displays. Their advantages, such as planar light emission characteristics, flexible and bendable design, low driving voltage and environmental friendliness, make them highly promising for future development.[1] Achieving efficient and stable WOLEDs relies on the coordinated action of multiple luminescent components.[2] Currently, mainstream technical routes include two main categories: first, a multi-layered luminescent stack structure realizes white light by vertically stacking red, green, and blue primary color luminescent layers; second, single-layer luminescence is achieved by a co-doping system, where multiple fluorescent or phosphorescent dyes are doped in a single host material.[3] Although the two aforementioned schemes have achieved commercial application, they still face challenges, including complex structures, severe degradation in efficiency, and insufficient chromatic stability. Furthermore, traditional fluorescent or phosphorescent hybrid systems are limited by the high cost of precious metals and the instability of blue light materials, while all-fluorescent systems based on three primary colors face the challenge of low utilization rates of triplet excitons.[4] In particular, the dependence of traditional WOLEDs on deep-blue light materials creates a fundamental contradiction between efficiency and lifetime.[5]

In recent years, exciplex-based white light systems have emerged as a promising third approach to address the aforementioned contradictions. These systems can cover the entire visible light spectrum through complementary color luminescence, and do not rely on precious metals for the exciton regulation process. An exciplex is a transient complex arising from a charge-transfer (CT) state formed at the interface of two different molecules in the excited state. Its broad-spectrum emission, characterized by a full width at half maximum (FWHM) greater than 150 nm, is attributed to the unique energy level structure of its CT state.[6] This phenomenon enables a simpler device structure, while providing multiple advantages in exciton utilization, spectral regulation and cost reduction, serving as an important driving force for the industrialization of WOLEDs. From the perspective of healthy lighting, exciplex-based white light devices have an inherent advantage in

[a]Shanxi University of Electronic Science and Technology, Linfen 041000, China
[b]College of Materials Science and Engineering, Taiyuan University of Technology, Taiyuan 030024, China. E-mail: wuyuling@tyut.edu.cn; miaoyanqin@tyut.edu.cn
[c]Department of Mechanical and Electrical Engineering, Shanxi Institute of Energy, Jinzhong 030600, China

reducing blue light hazard. Compared to conventional LEDs, the electroluminescent (EL) spectra of these devices exhibit a substantially lower intensity of the high-energy blue light component in the range 400–430 nm.[7] The mCP:pTPOTZ[8] system reported by Xu Hui's research group completely avoids the deep-blue light band during white light emission, maintaining a stable color temperature of around 3000 K. This characteristic not only meets general lighting requirements but also significantly reduces the risk of retinal photochemical damage, thereby providing a material basis for eye-friendly lighting.[9]

In addition, exciplex-based white light devices have been successfully applied in both vacuum evaporation and wet spin-coating processes. The mCP:PO-T2T[10] type exciplex system deposited by a vacuum process can strongly confine the carrier recombination region within the interface at the nanoscale by precisely controlling the thickness of the luminescent layer, thereby increasing the proportion of exciplex emission to over 70%. In the solution-processed device, white light emission with a high color rendering index (CRI) of 85 was achieved through a blended interface formed between the polymer blue light material F8BT[11] and the metal oxide electron transfer layer (ETL) composed of ZnO nanoparticles. This was accomplished even with a nominal thickness of 20 nm, as the effective exciplex region diffused to a depth of 15 nm due to solvent-induced molecular miscibility.[12]

The performance of devices is highly dependent on the fabrication process, which is a critical variable determining the outcome. Therefore, we designed a type of luminescent material with exceptional compatibility for both vacuum evaporation and solution processing. This material can form an exciplex to achieve single-molecule white light emission, offering unparalleled versatility.

In this work, an aniline-based carbazole derivative, *N*-(4-aniline) carbazole (CzPAF), with unique rigidity and electron-donating properties, is selected as the core to design two completely symmetrical D–π–D′–π–D-type blue light small-molecule luminescent materials, **CzPAF-DPA** and **CzPAF-DF**, based on 9,9-dioctylfluorene with better solubility as a π bridge and peripheral groups with different degrees of conjugation. The optimized structures indicate that both molecules form a vertical spatial configuration between their peripheral substituent groups and the fluorene unit, which can reduce π–π stacking between molecules and improve luminescence properties. In non-doped evaporated devices, both materials exhibited exciplexes at 500 nm at the interface between the light-emitting layer (EML) and the electron transport layer (ETL).[13,14] Furthermore, by adjusting the thickness of the light-emitting layer **CzPAF-DPA**, a controllable transition from single-molecule warm white light to cold white light emission was achieved in both evaporation-deposited and wet spin-coated devices. This research provides a crucial theoretical basis for the development of multi-process compatible blue light devices, and promotes the practical application of OLED technology in the field of printed displays.[15]

2 Results and discussion

2.1 Synthesis and characterization

We targeted the synthesis of **CzPAF-DPA** and **CzPAF-DF** (Fig. 1) by linking CzPAF-Br with different peripheral groups of varying degrees of conjugation, 4,4′-dimethoxydiphenylamine and *N*-(4-methoxyphenyl)-9,9-dimethyl-9H-fluoren-2-amine, as donors through Buchwald–Hartwig amination. Both products were purified and recrystallized, and the structures and purities of the intermediates and both target products were characterized using ^{1}H NMR, ^{13}C NMR and are displayed in SI.

2.2 Photophysical property and thermal stability

As shown in Fig. 2, the photophysical properties of **CzPAF-DPA** and **CzPAF-DF** were investigated with UV-vis spectra and PL spectra in different states of dilute solution and thin film.[16] The corresponding data are summarized in Table 1. The maximum absorption peaks of **CzPAF-DPA** and **CzPAF-DF** in dilute toluene solution were at 397 and 403 nm, respectively, which were attributed mainly to the intramolecular n–π* transition, and their corresponding maximum emission peaks were at 420 and 425 nm. The slight redshift of 5 nm observed in the emission peak of **CzPAF-DF**, compared to **CzPAF-DPA**, is likely attributed to the extended conjugation provided by its peripheral methylfluorene groups compared to that of methoxybenzene. In the thin-film state (Fig. 2b), the UV-vis absorption spectra of both materials exhibited similar photophysical properties, remaining fairly consistent with those in solution, accompanied by a redshift of only 3 nm. Their PL spectra located at 430 and 432 nm in the blue light band were also slightly redshifted, arising from the enhancement of the intermolecular interactions.[17–19] In comparison, the emission spectra of **CzPAF-DF** exhibited minimal change between solution and film, probably due to the increased steric hindrance caused by the larger peripheral group methylfluorene. In addition, **CzPAF-DF** also showed a higher fluorescence quantum yield (Φ_{PL}) of 69.0% in toluene solution compared to that for **CzPAF-DPA** of 61.3%, which was determined by fluorenyl groups with high fluorescence quantum efficiency. The thermal stability of the two materials, **CzPAF-DPA** and **CzPAF-DF** (Fig. 2c), under a nitrogen atmosphere was revealed by TGA analysis, with 5% weight loss decomposition temperatures (T_d) of 408 and 418 °C, respectively, which are favorable for the preparation of OLED devices. Their glass transition temperatures (T_g) in DSC are 76 and 93 °C, respectively.[20] The better thermal stability of **CzPAF-DF** is attributed to the extended conjugation structure of 9,9-dimethylfluorene compared to methoxybenzene, which enhances the molecular rigidity. To further confirm the excited-state nature of the compounds, the solvatochromic properties of **CzPAF-DPA** and **CzPAF-DF** in various solvents with different polarities were examined. The UV absorption spectra of **CzPAF-DPA** and **CzPAF-DF** remain unchanged in solvents of varying polarity (Fig. 2d and g). Thus, their PL spectra (Fig. 2e and h) show a bathochromic shift with successively increased polarity from low-polarity *n*-hexane ($f = 0.0012$) to high-polarity acetonitrile ($f = 0.305$). The redshift of 19 nm for **CzPAF-DPA** is

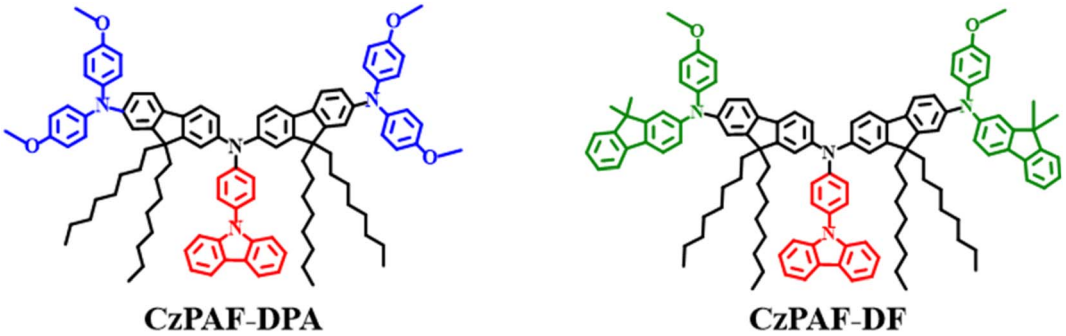

Fig. 1 Chemical structures of CzPAF-DPA and CzPAF-DF.

greater than that for **CzPAF-DF** with the narrowest spectral shift of 13 nm, showing that **CzPAF-DPA** is dominated by CT state character, while **CzPAF-DF** behaves with a more locally excited (LE) state character.[21] The transient PL decay spectra of **CzPAF-DPA** and **CzPAF-DF** neat films were measured to provide deep insight into the excited-state properties. Both compounds exhibited double-exponential decay with fitted lifetimes of 0.32/3.83 and 0.30/2.45 ns, respectively (Fig. 2f), manifesting the two radiative decay pathways. This suggests that their emission originates primarily from the LE state character, accompanied by a smaller proportion of CT character, which is also consistent with the solvation effect.[22]

Afterwards, we tested the electrochemical properties of **CzPAF-DPA** and **CzPAF-DF** using an electrochemical

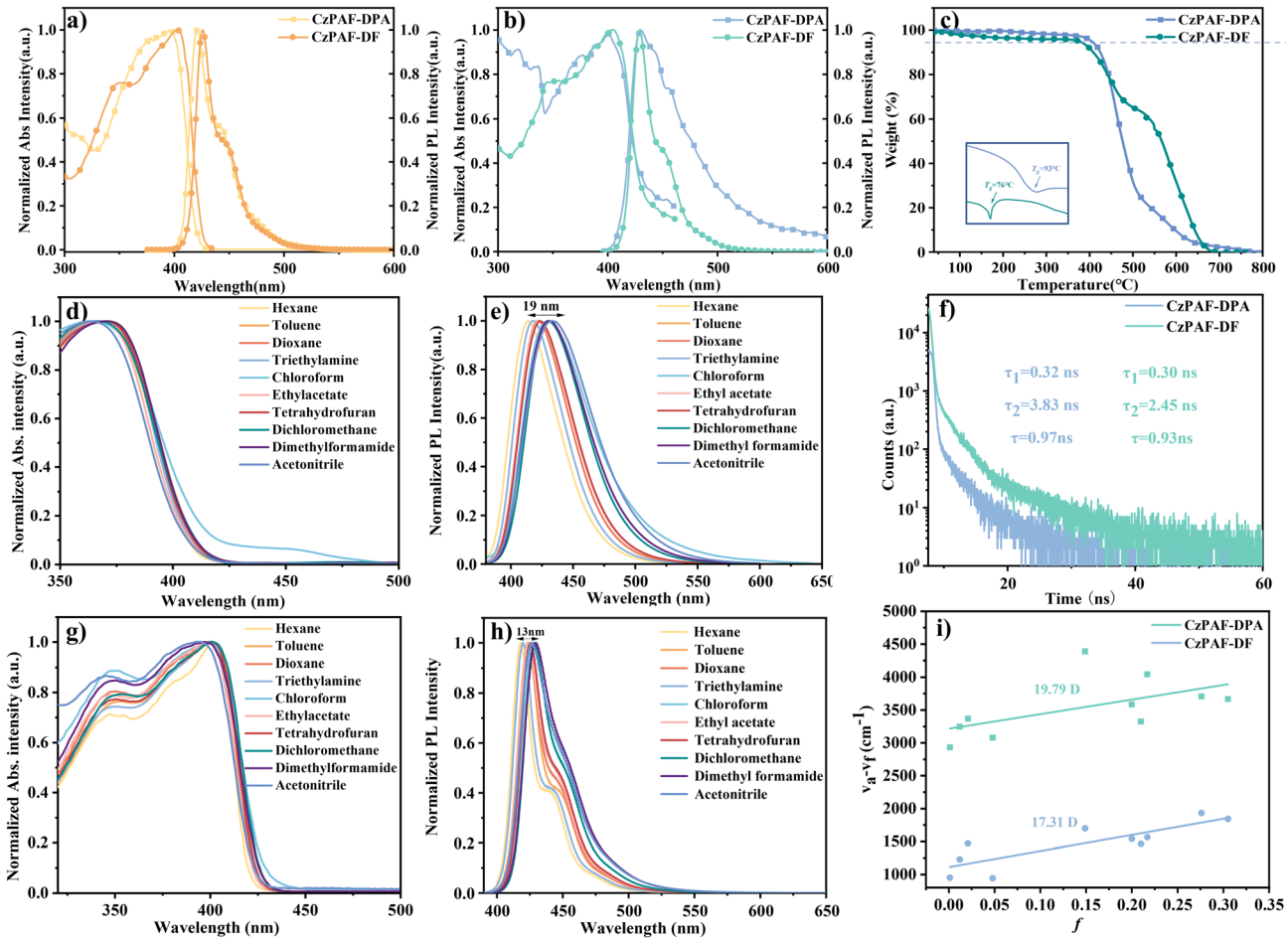

Fig. 2 UV-vis spectra and PL spectra of CzPAF-DPA and CzPAF-DF in toluene solution (1×10^{-5} M) (a) and thin film (b); TGA and DSC (c) curves; UV-vis spectra and PL spectra of CzPAF-DPA (d and e) and CzPAF-DF (g and h) in different polar solvents; (f) transient PL decay spectra; (i) fitted correlation of the Stokes shift as a function of solvent polarity.

Table 1 The physical properties of CzPAF-DPA and CzPAF-DF

Compounds	T_d/T_g [°C]	$\lambda_{abs,sol}$ [nm]	$\lambda_{pl,sol}$ [nm]	$\lambda_{abs,film}$ [nm]	$\lambda_{pl,film}$ [nm]	E_g [eV]	Φ_{PL} [%]	HOMO/LUMO [eV]
CzPAF-DPA	408/76	397	420	400	430	2.89	61.3	−5.36/−2.47
CzPAF-DF	418/93	403	425	406	432	2.87	69.0	−5.43/−2.56

workstation under a nitrogen atmosphere at room temperature, and cyclic voltammetry curves (CV curves) of the two materials were obtained, as shown in Fig. S9; the corresponding data are summarized in Table 1. The oxidation potentials E_{ox} of **CzPAF-DPA** and **CzPAF-DF** were 0.86 V and 0.93 V, respectively; the HOMO of **CzPAF-DPA** was −5.36 eV and that of **CzPAF-DF** was −5.43 eV, according to eqn (S2). Based on the absorption sidebands at 429 nm and 432 nm in the UV absorption spectra for **CzPAF-DPA** and **CzPAF-DF** in solution in Fig. 2, the **CzPAF-DPA** and **CzPAF-DF** band gaps, $E_g = 2.89$ eV and $E_g = 2.87$ eV, were calculated from eqn (S1). Then, using the HOMO energy levels and optical band gap E_g of **CzPAF-DPA** and **CzPAF-DF**, we can obtain the LUMO energy levels of **CzPAF-DPA** and **CzPAF-DF** as −2.47 eV and −2.56 eV, respectively, and the degree of conjugation of **CzPAF-DF** increases with respect to that of **CzPAF-DPA**, so that its HOMO and LUMO change, and the molecular degree of conjugation changes the chemical properties of the material.

2.3 Molecular ground and excited-state simulation calculations

To further investigate the optimized molecular geometrical structure and frontier orbital electron distributions of **CzPAF-DPA** and **CzPAF-DF**, their theoretical calculations were executed by density-functional theory (DFT) using the Gaussian 09 program on the 6-31G(d) basis group using the B3LYP algorithm. As shown in Fig. 3a, **CzPAF-DPA** has a three-dimensional stereo-configuration with three faces formed by the central N atom at a dihedral angle of about 120°, which is similar to that for **CzPAF-DF** with a identical dihedral angle (Fig. 3c). The peripheral substituents in both materials produce a perpendicular spatial configuration relative to the π-bridge fluorene.[23] The distorted molecular configuration reduces the intermolecular π–π stacking, which is favorable for luminescence properties. Meanwhile, the lowest unoccupied molecular orbital (LUMO) energy levels of **CzPAF-DPA** and **CzPAF-DF** are observed to be mainly distributed on the fluorene group, with minimal distribution on the other parts. The corresponding highest occupied molecular orbital (HOMO) energy levels are mainly localized on molecular fragments other than the carbazole unit, while the HOMO and LUMO produce partial overlap at the π-bridge fluorene, accompanied by partial spatial separation between the donor and acceptor groups.

To deepen understanding of the excited states, the electron-leap features of the excited single states (S_1–S_m) and the triplet states (T_1–T_n) of **CzPAF-DPA** and **CzPAF-DF** were analyzed by simulating the natural transition orbitals (NTOs) with electron- and hole-orbital in a NOT pair, as shown in Fig. 3(b and d). In single states, the hole and electron distributions of **CzPAF-DPA** and **CzPAF-DF** exhibit similar characteristics.[24] The separation of hole and electron distributions of **CzPAF-DPA** in the S_1 state shows a charge-transfer (CT) state character with completely separated holes and electrons, while **CzPAF-DF** in the S_1 state presents a locally excited (LE) state character with fully overlapping holes and electrons. Furthermore, the S_1 state energy for **CzPAF-DF** of 2.31 eV is slightly lower than that for **CzPAF-DPA** of 2.41 eV, resulting in a slight redshift of the PL emission spectrum. In the S_2 state, the holes of both **CzPAF-DPA** and **CzPAF-DF** are distributed mainly on the peripheral groups of one side and π bridges, whereas the electrons of both molecules are distributed only on the π bridges, in which the partial overlap exhibits a weak hybrid local and charge-transfer (HLCT) state character from hole to electron. The triplet states of **CzPAF-DPA** remain fairly consistent from hole to electron to exhibit an LE state characteristic, indicating a completely different distribution character from those in the corresponding singlet states, which is conducive to the radiative exciton transition and the improved exciton utilization. For **CzPAF-DF**, we replaced methylfluorene in the peripheral group to extend the conjugation, resulting in a partial overlap from hole to electron.[25]

2.4 Electroluminescent properties

To test the electroluminescence (EL) performance of both blue light-emitting materials, we designed and prepared three-layer structured non-doped devices as ITO/M_OO_3 (3 nm)/NPB (40 nm)/TCTA (10 nm)/**CzPAF-DPA** (Device I) and **CzPAF-DF** (Device II) (30 nm)/TPBi (40 nm)/LiF (1 nm)/AL (120 nm), as shown in Fig. 4a. In this device, ITO was used as the anode; TCTA (4,4′4′-tris(*N*-carbazolyl)-triphenylamine) as the hole-transporting layer (HTL); TPBi (1,3,5-tris(*N*-phenylbenzimidazol-2-yl)benzene) as the electron-transporting layer (ETL) and hole-blocking layer; and LiF/Al as the cathode. The key properties of these devices are summarized in Table S1.

The EL spectra of **CzPAF-DPA** and **CzPAF-DF** (Fig. 4b and c) at different voltages both showed two emission peaks around 425 and 500 nm. Compared with their PL spectra, the narrow blue light emission peaks near 425 nm for **CzPAF-DPA** and **CzPAF-DF** should originate from the monomer emission of the luminescent molecule. The wider green light emission peaks at 600 nm appear only in the EL spectra, which might be attributed to the generation of an exciplex between the light-emitting layer and the ETL (TPBi). The significant differences in LUMO energy level between the two molecules and TPBi (0.47 eV and 0.14 eV, respectively) create substantial energy barriers for electron injection into the light-emitting layer. This forces electrons to accumulate at the interface, leading to exciplex formation. The exciplex emission peaks of both **CzPAF-DPA** and **CzPAF-DF** were observed with higher initial intensity, which gradually

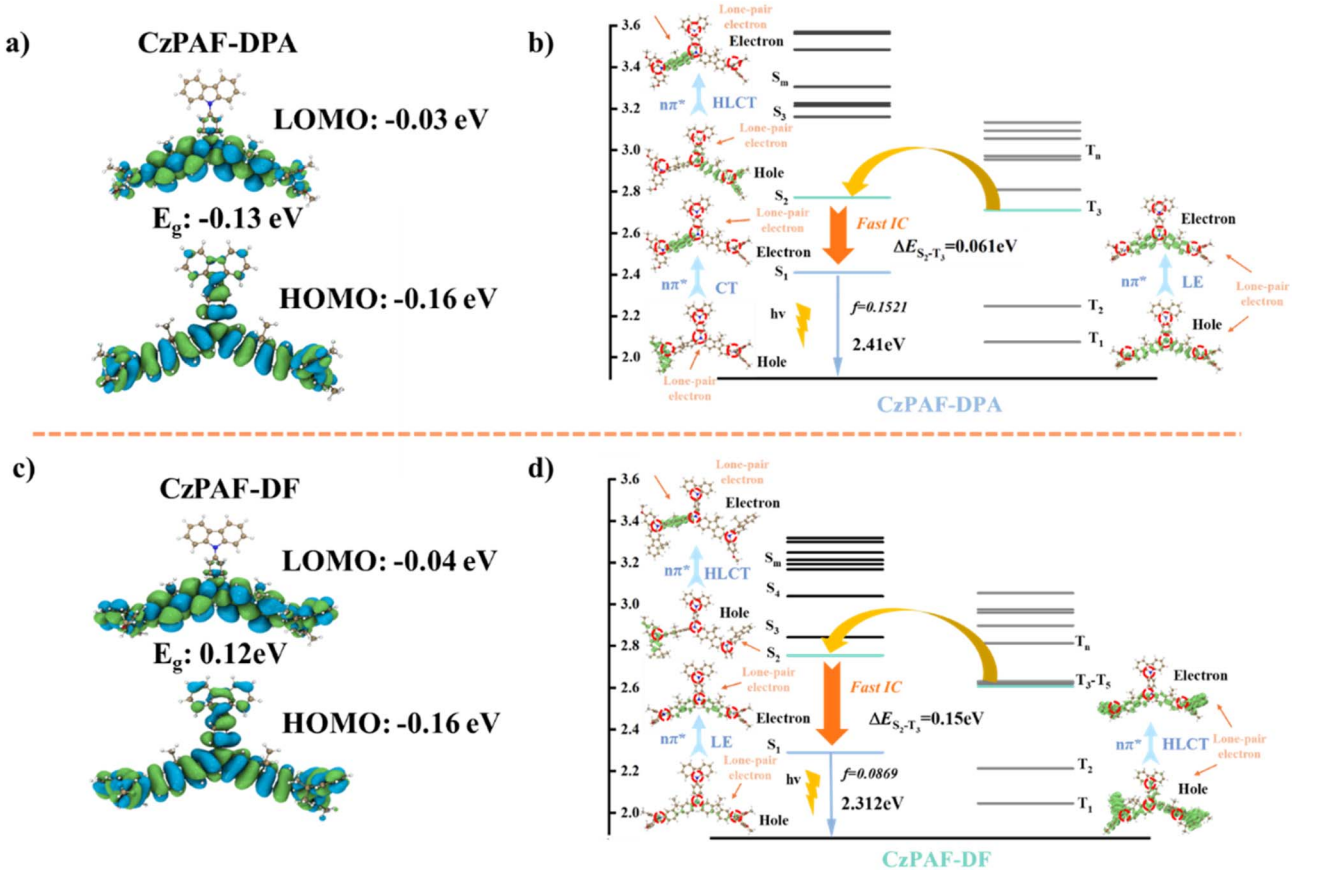

Fig. 3 Optimized molecular structures, LUMO and HOMO spatial distributions (a and c) and singlet and triplet energy diagrams (b and d) of CzPAF-DPA and CzPAF-DF.

decreased with increasing driving voltage. This quenching of exciplex emission occurred while the intensity of blue light remained constant.[26] This is because the injection rates of electrons and holes are relatively low at low voltages, which facilitates the formation of balanced charge carriers at the interface between the light-emitting layer and the electron transport layer, which is conducive to efficient exciplex generation. As the voltage increases, enhanced carrier injection allows more holes and electrons to overcome the potential barrier between the interfaces and enter the light-emitting layer, resulting in decreased carrier concentration at the interface and the weakened emission peak of the exciplex. Although the generation of the exciplex has a great impact on the EL spectra, the intrinsic luminescence peaks of **CzPAF-DPA** and **CzPAF-DF** are similar to those of the thin-film luminescence peaks, with a slight blueshift of $\approx$5 nm, which is attributed to the larger distorted steric hindrance, which effectively suppresses the intermolecular π–π stacking by introducing a larger core structure, CzPAF. In order to confirm that the exciplex is generated by the light-emitting layer and the electron transport layer, we selected **CzPAF-DPA** with a high intensity of the exciplex as an example to investigate the PL spectra after doping it with the electron transport material TPBi (Fig. S10), and the emission peak observed at 500 nm confirms the above results.[27] Broad-spectrum green light and blue light can be combined to produce white light. Nevertheless, white light could not be achieved due to the insufficient intensity of the exciplex for **CzPAF-DPA** in Fig. 4b. According to the formation mechanism of the exciplex, reducing the thickness of the luminescent layer can regulate the emission intensity of the exciplex, thereby achieving white light emission. Therefore, based on the above luminescent characteristics, we fabricated light-emitting devices with the same structure and luminescent layers of 20 and 10 nm, respectively. It can be clearly seen from Fig. 4d and e that the intensity of the exciplex peaks gradually increases as the thickness of the luminescent layer decreases, and the EL spectra can be controllably regulated from warm white light to cold white light under the action of an electric field when the thickness of the luminescent layer is reduced to 10 nm. This is because the diffusion distance of excitons in thicker EMLs between the luminescent layer and the electron transfer layer is limited, resulting in lower luminescence intensity for the generated exciplex.[28] When the EML is very thin, excitons generated at any position within the EML are extremely close to the ETL interface, which makes the exciton energy more likely to be transferred to the molecular pairs at the interface, thereby promoting the formation and luminescence of an exciplex. Hence, a thin EML can shorten the distance of energy transfer, thereby improving the efficiency of energy transfer.

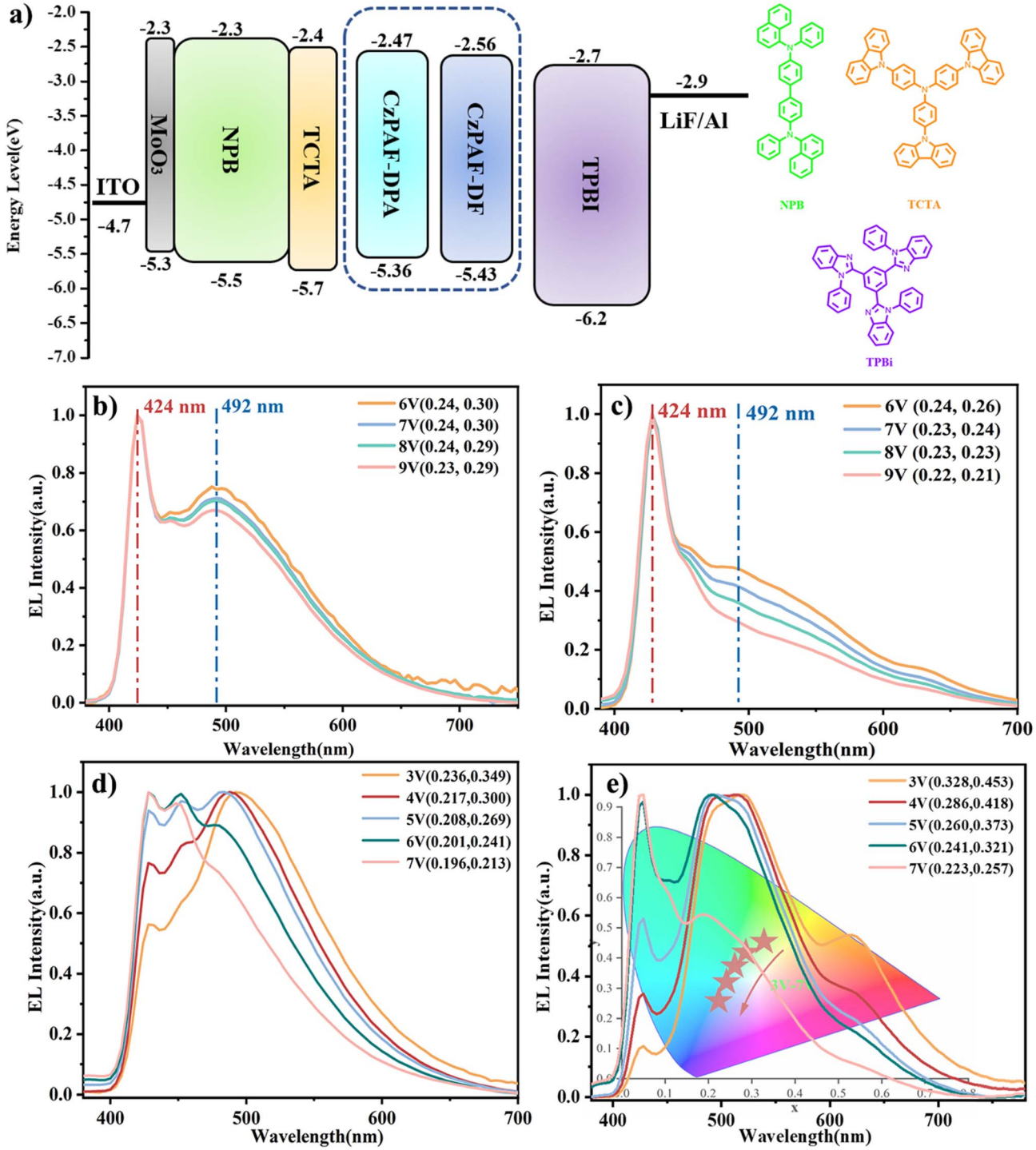

Fig. 4 (a) Device energy level structure, EL spectra of CzPAF-DPA (b, 30 nm), CzPAF-DF (c, 30 nm), CzPAF-DPA (d, 20 nm) and CzPAF-DPA (e, 10 nm) at different voltages.

Large-area flexible lighting is the future trend. Hence, we fabricated devices based on **CzPAF-DPA** using wet spin-coating by varying the concentration of EML to achieve large-area lighting in future commercial applications due to the presence of 9,9-dioctyloxyfluorene. The device structure is ITO/PEDOT:PSS/TPD/EML/TPBI (50 nm)/LIF (1 nm)/Al (120 nm). We set the concentration of the EML luminescent layer as A – 20 mg mL^{-1}, B – 30 mg mL^{-1}, C – 40 mg mL^{-1}, D – 50 mg mL^{-1}, respectively. As shown in Fig. 5, the EL spectra with different concentrations for the luminescent layer all produced an emission peak for the exciplex at 500 nm. These results further confirm the electric-field-induced interfacial interaction between the luminescent layer and the electron transport layer TPBi. Simultaneously, the intensity of the exciplex emission peak increases with the thickness of the light-emitting layer, which is opposite to the EL spectral trend in the evaporated

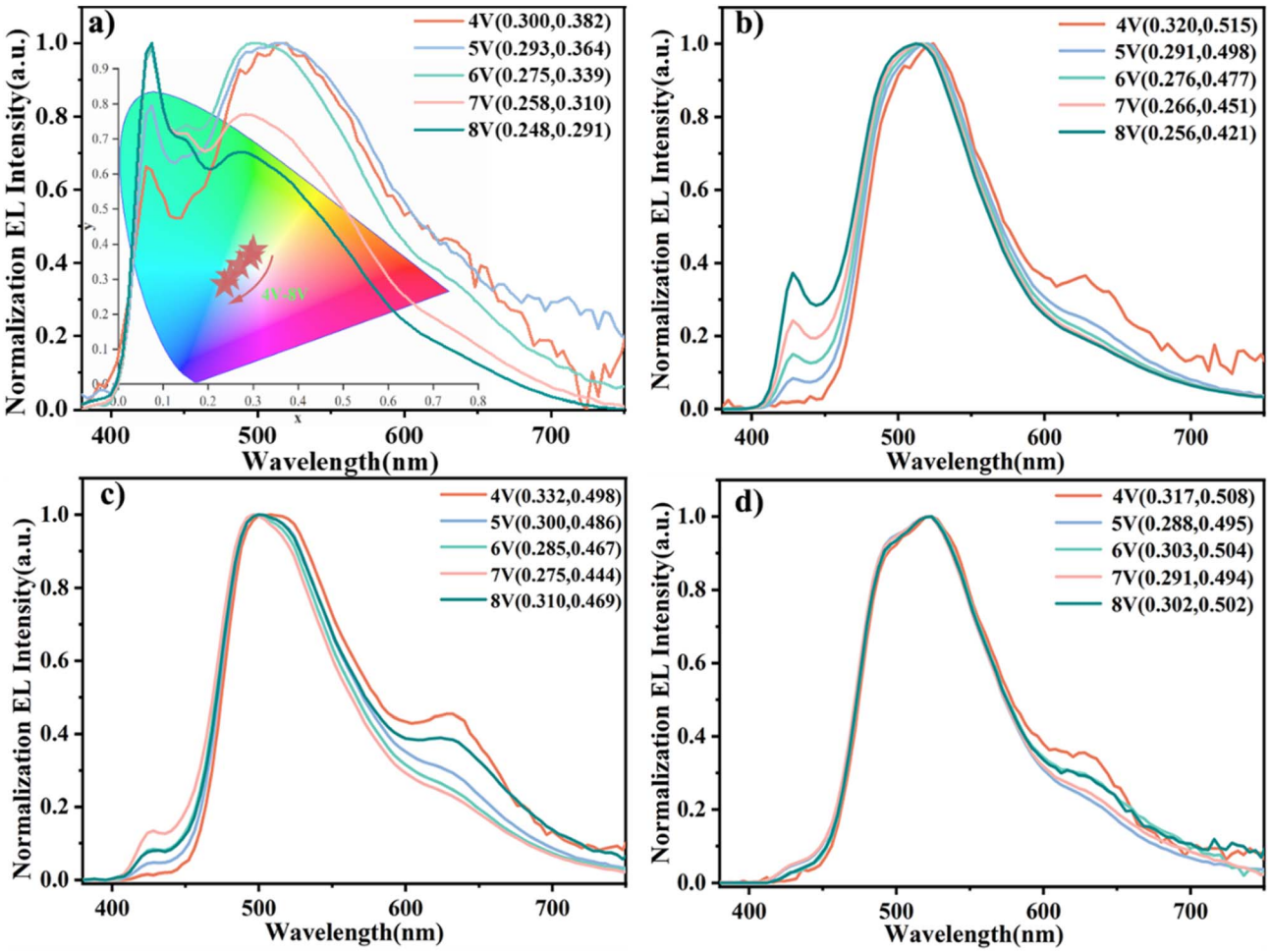

Fig. 5 EL spectra of CzPAF-DPA-based devices: (a) EML (20 mg mL^{-1}), (b) EML (30 mg mL^{-1}), (c) EML (40 mg mL^{-1}), (d) EML (50 mg mL^{-1}).

devices.[29] This is because the solvent residue effect in the spin-coating process promotes intermolecular miscibility at the interface, increasing the emission intensity of the excited complex by a factor of nearly two, and causing a slight redshift in the spectrum. In the thinner light-emitting layer, the injection of electrons and holes usually occurs near the interface between the electron transport layer and the light-emitting layer, resulting in carrier recombination within a highly confined region. When the light-emitting layer becomes thicker, electrons and holes have more space to transport and diffuse. This is because the solvent remains longer, forming a wider mixing zone at the interface. As a result, they are no longer pinned at the injection interface and can penetrate deeper into the bulk of the light-emitting layer, where they encounter each other, enhancing the luminescence intensity. This significantly expands the effective spatial range for electron–hole encounters and exciplex formation. Furthermore, the emission peak of the luminescent layer itself at 425 nm disappeared when the luminescent layer was 50 mg mL^{-1}, which may be due to the increase in carrier migration distance due to the increase in the thickness of the luminescent layer and the significant decrease in carrier complexation efficiency, leading to the disappearance of the blue light emission.[30] Fortunately, a **CzPAF-DPA** device based on 20 mg mL^{-1} solution concentration similarly achieved dynamic control from warm white light to cool white light, while the blue light itself also maintained relatively high intensity. In brief, the above results demonstrate that the exciplex emission intensity can be modulated by adjusting the thickness of the light-emitting layer, thereby enabling precise regulation over the overall emission color.

3 Conclusions

Two D–π–D′–π–D-type blue light materials, **CzPAF-DPA** and **CzPAF-DF**, based on a core aniline-based carbazole and 9,9-dibutylfluorene as a π bridge with two peripheral donors with different degrees of conjugation, were successfully synthesized by Buchwald–Hartwig amination. Both materials exhibit blue light emission and good thermal stability with thermal decomposition temperatures (T_d) of 408 and 418 °C, respectively. The electroluminescence spectra of **CzPAF-DPA** and **CzPAF-DF** both represented broad-band emission with two main emission peaks located at 424/428 nm for the intrinsic emission peak of blue light materials, and 496/500 nm for the exciplex generated at the interface between the light-emitting layer and the electron transport layer. By varying the EML

thickness, we achieved dynamically tunable white light emission from warm to cool color temperature in **CzPAF-DPA**-based devices fabricated by both processes of wet spin-coating and vacuum evaporation. The generated exciplex achieves single-molecule white light emission, and it shows significant potential for application in future flexible lighting and health-conscious lighting scenarios.

Conflicts of interest

There are no conflicts to declare.

Data availability

Data available on request from the authors. The data that support the findings of this study are available from the corresponding author, [Yuling Wu], upon reasonable request. Supplementary information: the experimental section, NMR spectra of products and intermediates, and CV curves. See DOI: **https://doi.org/10.1039/d5ra04330a**.

Acknowledgements

This work was financially supported by the National Natural Science Foundation of China (6207031407, 62074109), the Joint Funds of the National NSFC (U21A20492), Shanxi Province Natural Science Foundation (202103021224076, 202203021211284), Science and Technology Innovation Talent Team Project of Shanxi Province (202204051001013).

References

1 C. Adachi, M. A. Baldo, M. E. Thompson and S. R. Forrest, *J. Appl. Phys.*, 2001, **90**, 5048–5051, DOI: **10.1063/1.1409582**.
2 S. R. Forrest, D. D. C. Bradley and M. E. Thompson, *Adv. Mater.*, 2003, **15**, 1043–1048, DOI: **10.1002/adma.200302151**.
3 I. R. D. Moraes, S. Scholz, B. Lüssem and K. Leo, *Org. Electron.*, 2011, **12**, 341–347, DOI: **10.1016/j.orgel.2010.11.004**.
4 Y. Zhang, J. Lee and S. R. Forrest, *Nat. Commun.*, 2014, **5**, 5008, DOI: **10.1038/ncomms6008**.
5 H. Nakanotani, T. Higuchi, T. Furukawa, K. Masui, K. Morimoto, M. Numata, H. Tanaka, Y. Sagara, T. Yasuda and C. Adachi, *Nat. Commun.*, 2014, **5**, 4016, DOI: **10.1038/ncomms5016**.
6 Z. Xu, B. Z. Tang, Y. Wang and D. Ma, *J. Mater. Chem. C*, 2020, **8**, 2614–2642, DOI: **10.1039/C9TC06441A**.
7 V. V. Patil, K. H. Lee and J. Y. Lee, *J. Mater. Chem. C*, 2020, **8**, 3051–3057, DOI: **10.1039/C9TC06434F**.
8 X. Zhan, Z. Wu, Y. Gong, J. Tu, Y. Xie, Q. Peng, D. Ma, Q. Li and Z. Li, *Research*, 2020, **2020**, 8649102, DOI: **10.34133/2020/8649102**.
9 A. Endo, K. Sato, K. Yoshimura, T. Kai, A. Kawada, H. Miyazaki and C. Adachi, *Appl. Phys. Lett.*, 2011, **98**, 83302, DOI: **10.1063/1.3558906**.
10 J. Liang, T. Wu and J. Chen, *J. Electron. Mater.*, 2023, **52**, 5013–5021, DOI: **10.1007/s11664-023-10470-2**.
11 M. Mamada, R. Komatsu and C. Adachi, *ACS Appl. Mater. Interfaces*, 2020, **12**, 28383–28391, DOI: **10.1021/acsami.0c05449**.
12 H. Uoyama, K. Goushi, K. Shizu, H. Nomura and C. Adachi, *Nature*, 2012, **492**, 234–238, DOI: **10.1038/nature11687**.
13 D. Zhang, M. Cai, Y. Zhang, D. Zhang and L. Duan, *Mater. Horiz.*, 2016, **3**, 145–151, DOI: **10.1039/C5MH00258C**.
14 S. Youn Lee, T. Yasuda, H. Nomura and C. Adachi, *Appl. Phys. Lett.*, 2012, **101**, 93306, DOI: **10.1063/1.4749285**.
15 S. Hirata, Y. Sakai, K. Masui, H. Tanaka, S. Y. Lee, H. Nomura, N. Nakamura, M. Yasumatsu, H. Nakanotani, Q. Zhang, K. Shizu, H. Miyazaki and C. Adachi, *Nat. Mater.*, 2015, **14**, 330–336, DOI: **10.1038/nmat4154**.
16 Y. Kondo, K. Yoshiura, S. Kitera, H. Nishi, S. Oda, H. Gotoh, Y. Sasada, M. Yanai and T. Hatakeyama, *Nat. Photonics*, 2019, **13**, 678–682, DOI: **10.1038/s41566-019-0476-5**.
17 C. Chiang, A. Kimyonok, M. K. Etherington, G. C. Griffiths, V. Jankus, F. Turksoy and A. P. Monkman, *Adv. Funct. Mater.*, 2013, **23**, 739–746, DOI: **10.1002/adfm.201201750**.
18 J. Hu, Y. Pu, F. Satoh, S. Kawata, H. Katagiri, H. Sasabe and J. Kido, *Adv. Funct. Mater.*, 2014, **24**, 2064–2071, DOI: **10.1002/adfm.201302907**.
19 W. Zeng, Y. Zhao, W. Ning, S. Gong, Z. Zhu, Y. Zou, Z. H. Lu and C. Yang, *J. Mater. Chem. C*, 2018, **6**, 4479–4484, DOI: **10.1039/C8TC00317C**.
20 W. Liu, S. Ying, R. Guo, X. Qiao, P. Leng, Q. Zhang, Y. Wang, D. Ma and L. Wang, *J. Mater. Chem. C*, 2019, **7**, 1014–1021, DOI: **10.1039/C8TC05707A**.
21 B. Li, G. Tang, L. Zhou, D. Wu, J. Lan, L. Zhou, Z. Lu and J. You, *Adv. Funct. Mater.*, 2017, **27**, 1605245, DOI: **10.1002/adfm.201701181**.
22 F. Liu, Z. Cheng, L. Wan, L. Gao, Z. Yan, D. Hu, L. Ying, P. Lu and Y. Ma, *Chem. Eng. J.*, 2021, **426**, 131351, DOI: **10.1016/j.cej.2021.131351**.
23 H. Zhang, J. Xue, C. Li, S. Zhang, B. Yang, Y. Liu and Y. Wang, *Adv. Funct. Mater.*, 2021, **31**, 2100704, DOI: **10.1002/adfm.202100704**.
24 W. Cui, C. Liu, X. Chao, M. Xie, Q. Sun, D. Liu, Y. Pan, S. Zhang, S. Xue and W. Yang, *Adv. Opt. Mater.*, 2023, **11**, 2202947, DOI: **10.1002/adom.202202947**.
25 K. H. Kim, S. Lee, C. K. Moon, S. Y. Kim, Y. S. Park, J. H. Lee, J. Woo Lee, J. Huh, Y. You and J. J. Kim, *Nat. Commun.*, 2014, **5**, 4769, DOI: **10.1038/ncomms5769**.
26 S. H. Lee, T. Nakamura and T. Tsutsui, *Org. Lett.*, 2001, **3**, 2005–2007, DOI: **10.1021/ol010069r**.
27 X. Xie, J. Liu, H. Zhao, L. Yan, Y. Wu, Y. Miao and H. Wang, *RSC Adv.*, 2024, **14**, 34311–34319, DOI: **10.1039/D4RA05803H**.
28 J. J. Liang, Y. Li, Y. Yuan, S. H. Li, X. D. Zhu, S. Barlow, M. K. Fung, Z. Q. Jiang, S. R. Marder and L. S. Liao, *Mater. Chem. Front.*, 2018, **2**, 917–922, DOI: **10.1039/C7QM00605E**.
29 X. Qiu, S. Ying, C. Wang, M. Hanif, Y. Xu, Y. Li, R. Zhao, D. Hu, D. Ma and Y. Ma, *J. Mater. Chem. C*, 2019, **7**, 592–600, DOI: **10.1039/C8TC05469J**.
30 Z. Peng, S. Tao, X. Zhang, J. Tang, C. S. Lee and S. T. Lee, *J. Phys. Chem. C*, 2008, **112**, 2165–2169, DOI: **10.1021/jp074834g**.